Naval Surface Warfare Center
Carderock Division
West Bethesda, MD 20817-5700

NAVSEA
WARFARE CENTERS
Carderock Division

NSWCCD-50-TR–2012/001 April 2012
Hydromechanics Department Report

Nearshore Sea Clutter Measurements From A Fixed Platform

By
Erin E. Hackett, Anne M. Fullerton, Craig F. Merrill, and Thomas C. Fu

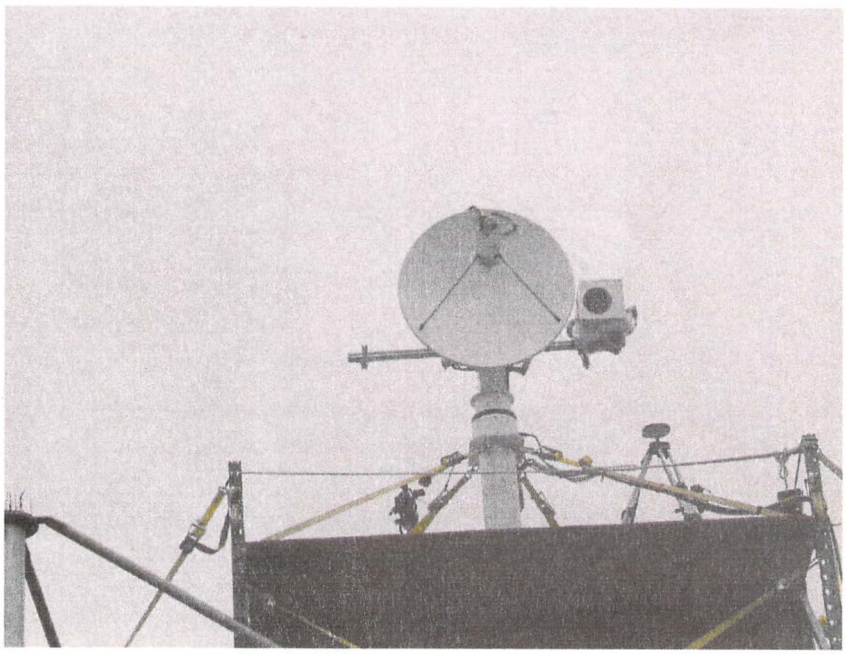

REPORT DOCUMENTATION PAGE

Form Approved
OMB No. 0704-0188

1. REPORT DATE *(DD-MM-YYYY)*	2. REPORT TYPE	3. DATES COVERED *(From - To)*
April 2012	Final	July 2010 - Dec 2011

4. TITLE AND SUBTITLE
Nearshore Sea Clutter Measurements from a Fixed Platform

5a. CONTRACT NUMBER
N0001411WX20753,N0001410WX211

5b. GRANT NUMBER

5c. PROGRAM ELEMENT NUMBER
0603236N

6. AUTHOR(S)

Erin E. Hackett, Anne M. Fullerton, Craig F. Merrill, and Thomas C. Fu

5d. PROJECT NUMBER

5e. TASK NUMBER

5f. WORK UNIT NUMBER
11-1-5800-363,10-1-5800-328

7. PERFORMING ORGANIZATION NAME(S) AND ADDRESS(ES) AND ADDRESS(ES)

Naval Surface Warfare Center
Carderock Division
9500 Macarthur Boulevard
West Bethesda, MD 20817-5700

8. PERFORMING ORGANIZATION REPORT NUMBER

NSWCCD-50-TR-2012/001

9. SPONSORING / MONITORING AGENCY NAME(S) AND ADDRESS(ES)
Dr. Paul E. Hess III, Office of Naval Research
One Liberty Center
875 N. Randolph Street
Suite 1425
Arlington, VA 22203-1995

10. SPONSOR/MONITOR'S ACRONYM(S)
ONR

11. SPONSOR/MONITOR'S REPORT NUMBER(S)

12. DISTRIBUTION / AVAILABILITY STATEMENT Approved for public release; distribution unlimited.

13. SUPPLEMENTARY NOTES

14. ABSTRACT

This report describes a set of experiments performed in support of ONR's Environmental Sensing and Motion Forecast (ESMF) Program. The goal of the experiments was to obtain data to evaluate the ability of low-grazing angle radars to provide near-field, near-real time sea state data suitable for enabling a high-fidelity ship control system to control ship motion during Sea Basing ship-to-ship logistic operations in Sea State (SS) 4 and below. More specifically, the test evaluated the ability of radars to quantify characteristics of ocean waves via their radar cross-section (RCS) and Doppler signature. Measurements were performed using two different types of radar: a calibrated linear FM homodyne X- and Ku-band instrumentation radar (SCI, Inc., DREAM system), and an uncalibrated X-band navigation radar (Furuno) integrated with the WaMoS II® ocean monitoring system. Both radars were mounted at the end of the Scripps Institution of Oceanography (SIO) pier in La Jolla, CA, and measured ocean waves in a region approximately one nautical mile offshore. Another key component of this test

15. SUBJECT TERMS
Sea Clutter, Coherent Radar, Multipath, Sea State Measurements

16. SECURITY CLASSIFICATION OF:			17. LIMITATION OF ABSTRACT	18. NO. OF PAGES	19a. RESPONSIBLE PERSON
a. REPORT	b. ABSTRACT	c. THIS PAGE		21+vi	Erin Hackett
UNCLASSIFIED	UNCLASSIFIED	UNCLASSIFIED			19b. TELEPHONE NUMBER 301-227-5842

20120503008

14. ABSTRACT (continued)
was to obtain data to improve our understanding of ocean wave multipath physics, and explore means of improving the existing models for multipath signals generated by rough ocean surfaces. To meet these needs, the test also consisted of multipath measurements in addition to the sea clutter measurements. The former consisted of tests that measured the RCS of trihedrals mounted on a small boat, which varied the trihedrals' position in range and height, to provide a means of evaluating RCS from a known source and source location over a rough ocean surface. Independent measurements of the wave field were also performed using (i) an instrumented small boat positioned near the region being measured by the radars, (ii) miniature wave buoys deployed from the small boat, and (iii) by semi-permanent wave buoys operated in the vicinity of the test area. The wave climatology near the SIO pier was generally of low sea state with approximately unidirectional waves that contained contributions from both wind seas and swell. In addition, tide and wind data were collected at permanent environmental sensor stations located at the SIO pier. This report describes the instrumentation and experiments as well as provides examples of the acquired data, discussion on analysis plans, and some sample preliminary results.

CONTENTS

FIGURES

TABLES

INTERNATIONAL SYSTEM OF UNITS (SI) CONVERSION LIST

U.S. CUSTOMARY	METRIC EQUIVALENT
1 inch (in)	25.4 millimeter (mm), 0.0254 meter (m)
1 foot (ft)	0.3048 meter (m)
1 pound-mass (lbm)	0.4536 kilograms (kg)
1 pound-force (lbf)	4.448 Newtons (N)
1 foot-pound-force (ft-lbf)	1.3558 Newton-meters (N-m)
1 foot per second (ft/s)	0.3048 meter per second (m/s)
1 knot (kt)	1.6878 feet per second (ft/s) 0.5144 meter per second (m/s)
1 horsepower (hp)	0.7457 kilowatts (kW)
1 long ton (LT)	1.016 tonnes 1.016 metric tons 1016 kilograms (kg) 2240 pounds
1 inch water (60F)	248.8 Pascals (Pa)

ABSTRACT

This report describes a set of experiments performed in support of ONR's Environmental Sensing and Motion Forecast (ESMF) Program. The goal of the experiments was to obtain data to evaluate the ability of low-grazing angle radars to provide near-field, near-real time sea state data suitable for enabling a high-fidelity ship control system to control ship motion during Sea Basing ship-to-ship logistic operations in Sea State 4 and below. More specifically, the test evaluated the ability of radars to quantify characteristics of ocean waves via their radar cross-section and Doppler signature. Measurements were performed using two different types of radar: an SCI, Inc., DREAM calibrated linear FM homodyne X- and Ku-band instrumentation radar, and an uncalibrated Furuno X-band navigation radar integrated with the WaMoS II® ocean monitoring system. Both radars were mounted at the end of the Scripps Institution of Oceanography (SIO) pier in La Jolla, CA, and measured ocean waves in a region approximately one nautical mile offshore. Another key component of this test was to obtain data to improve our understanding of ocean wave multipath physics, and explore means of improving the existing models for multipath signals generated by rough ocean surfaces. To meet these needs, the test also consisted of multipath measurements in addition to the sea clutter measurements. The former consisted of tests that measured the RCS of trihedrals mounted on a small boat, which varied the trihedrals' position in range and height, to provide a means of evaluating RCS from a known source and source location over a rough ocean surface. Independent measurements of the wave field were also performed using (i) an instrumented small boat positioned near the region being measured by the radars, (ii) miniature wave buoys deployed from the small boat, and (iii) by semi- permanent wave buoys operated in the vicinity of the test area. The wave climatology near the SIO pier was generally of low sea state with approximately unidirectional waves that contained contributions from both wind seas and swell. In addition, tide and wind data were collected by permanent environmental sensor stations located at the SIO pier. This report describes the instrumentation and experiments as well as provides examples of the acquired data, discussion on analysis plans, and some sample preliminary results.

ACKNOWLEDGEMENTS

The authors would like to acknowledge the following people for their assistance during the field work: Eric Terrill and the other members of the Coastal Observing Research and Development Center at the Scripps Institution of Oceanography, Kristine Beale, Peter Stanton, Jesse Caldwell, and Don Wyatt from SAIC, Inc., and Richard Pokrass from Sensor Concepts, Inc. We would also like to thank Richard Pokrass for contributing several figures to this report. The authors would also like to recognize Andy Smith and Shaun Simmons, NSWCCD Code 70, for their participation and assistance with the tests. This research was supported by the Office of Naval Research under the direction of program manager Dr. Paul E. Hess III. We appreciate Dr. Hess' encouragement and support for this effort as well as that of his assistant, W. Rob Story (Fulcrum Corp.).

ADMINISTRATIVE INFORMATION

The work described in this report was performed by the Science and Technology Branch of the Resistance and Propulsion Division (Code 583) of the Hydromechanics Department at the Naval Surface Warfare Center, Carderock Division (NSWCCD). The work was performed under program element 0603236N, work requests N0001411WX20753 and N0001410WX21167, and work unit numbers 11-1-5800-363 and 10-1-5800-328.

INTRODUCTION

This report describes a set of experiments performed in support of the Office of Naval Research's Environmental Sensing and Motion Forecast (ESMF) Program. The primary objective of the experiments was to obtain data to evaluate the ability of low- grazing angle radars to provide near-field, near-real time sea state data suitable for enabling a high-fidelity ship control system to control ship motion during Sea Basing ship-to-ship logistic operations in Sea State (SS) 4 and below. More specifically, the test evaluated the ability of radars to quantify characteristics of ocean waves via their radar cross-section (RCS) and Doppler signature. Measurements were performed using two different types of radar: an SCI, Inc., DREAM calibrated linear FM homodyne X- and Ku-band instrumentation radar, and an uncalibrated Furuno X-Band navigation radar integrated with the WaMoS II® ocean monitoring system. Both radars were mounted at the end of the Scripps Institution of Oceanography (SIO) pier in La Jolla, CA, and measured ocean waves in a region approximately one nautical mile offshore. A subsequent effort performed a similar evaluation with the systems installed aboard the research vessel *MELVILLE*; a description of these tests is provided in a separate report.

The success of the ESMF program, as well as the execution of the Sea Basing mission, is predicated upon using accurate environmental sensor information to predict and control platform motion. An existing ocean wave measurement radar system, WaMoS II, requires periodic calibration using a local wave buoy to accurately quantify significant wave height [1]—a practice not suitable for ESMF applications. One of the potential factors associated with this shortcoming is insufficient treatment of multipath effects. Therefore, the secondary objective of these tests was to obtain data to improve our understanding of ocean wave multipath physics, and explore means of improving the existing models for multipath signals generated by rough ocean surfaces. To meet both objectives, the test involved sea clutter measurements as well as multipath measurements. The latter consisted of tests that measured the RCS of trihedrals mounted on a small boat, which varied the trihedrals' position in range and height, to provide a means of evaluating RCS from a known source and source location over a rough ocean surface. This report summarizes both parts of the experiments.

Both test objectives required independent measurements of the wave field. These measurements were performed using (i) an instrumented small boat positioned near the region being measured by the radars, (ii) miniature wave buoys deployed from the small boat, and (iii) semi-permanent wave buoys operated in the vicinity of the test area. The wave climatology near the SIO pier was generally of low sea state with approximately unidirectional waves that contained contributions from both wind seas and swell. In addition, tide and wind data were collected by permanent environmental sensor stations located at the SIO pier. This sea state and environmental data were needed to support both the sea clutter and multipath tests. For the former, development of algorithms and evaluation of radar performance for characterizing the wave field requires independent knowledge of the sea state for comparisons. It is important that more than one conventional source of wave data were collected because natural wave fields are not homogenous or stationary; thus, multiple sources of wave data provide a means of evaluating the spatial and temporal variability of the wave field. For multipath tests, characterization of the sea state is required to determine how multipath effects vary with sea state.

This document first describes the instrumentation used in the tests. Following this section, the sea-state, multipath and sea clutter measurements are each described in their respective sections, which include a description of the experiments along with sample results from preliminary post-processing of the data. The last section summarizes ongoing and future analysis plans.

INSTRUMENTATION

This section describes the various sensors deployed for these tests. Details regarding how the instrumentation was used for sea state, multipath, and sea clutter tests are discussed in their respective sections.

1. Vessel

A 7.6 m (25 ft) vessel, a Parker craft (hereafter referred to as the Parker) was used in various aspects of the tests including target mounting, wave buoy deployment, and sea state measurements. The vessel was operated by the SIO Coastal Observing Research and Development Center.

2. Senix Ultrasonic Distance Probes

Three Senix TSPC-15S-232 ultrasonic distance sensors were utilized. Each measured height above the water surface by measuring travel times of sound waves. They were setup in slave-master mode to reduce crosstalk between the sensors and sampled distance to the water surface at 20 Hz. Stated accuracy of the distance measurements is 0.25 mm for a maximum range of ±3 m. The nominal beamwidth of the Senix sensors is 12 degrees, which means that the sensor return may degrade when the relative angles between the surface and sensor orientation are more than 6 degrees. These limits were previously tested in the NSWCCD basin, and sensor signal was shown to drop out at angles greater than about 10 degrees. For the seas encountered during this test, this limit was not often exceeded, and any dropouts were removed prior to analysis. In addition, when the characteristic scales of the surface roughness are greater than the wavelength of the ultrasound frequency, there is a reduction in accuracy. The 3 Senix sensors were mounted on booms extending from the Parker. The configuration of these sensors on the Parker is shown in Figure 1. This Senix array measured height above the water at three different x, y, and z locations.

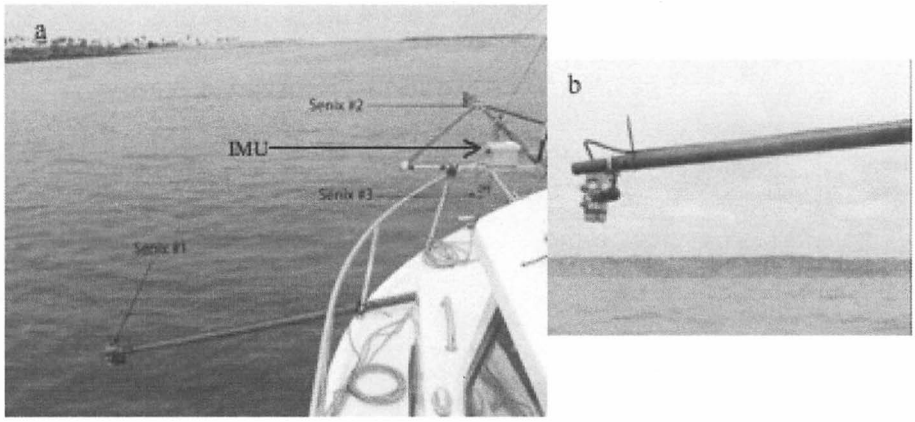

Figure 1. (a) Senix array and IMU. (b) Close-up of Senix ultrasonic distance sensor.

3. Inertial Measurement Unit

A Crossbow, model NAV440, inertial measurement unit (IMU), was installed aboard the Parker to measure its motion. This data was collected synchronously with the Senix measurements at 20 Hz. The IMU measured angular displacement (roll, pitch, and yaw), rotation rate, and acceleration with an accuracy of 0.02 deg, 0.02 deg s^{-1}, and 0.5 mg (milli-g), respectively. The corresponding maximum ranges were ±180 deg (±90 deg for pitch), ±200 deg s^{-1}, and ±4 g.

4. National Data Buoy Center (NDBC) Wave Buoys

Two permanent National Data Buoy Center (NDBC) buoys recorded wave data in the vicinity of the test area. These two NDBC buoys are #46231 and #46225, and are located at 32.748 deg north 117.370 deg west and 32.930 deg north 117.393 deg west, respectively. Both are Datawell Waverider® buoys, and the acquired data is available via the World Wide Web. However, due to effects of bottom topography and differences in location, the wave field at these buoys differed from that at the test site; thus, these measurements are only to be used in the event that the other two primary sources of wave data, provided by miniature wave buoys (see 5.) and Senix sensors (see 2.) are not available or unusable, and the data acquired by these buoys is not discussed further in this report.

5. SIO Miniature Directional Wave Buoys

The Scripps Institution of Oceanography designs and manufactures GPS-based miniature directional wave buoys. Two miniature buoys, #33 and #34, were used for these tests. One of the buoys is shown, close-up and deployed, in Figure 2. They measured water velocities, which were used to obtain sea surface elevation spectra using linear wave theory from which other wave statistics were computed. The one-dimensional (1-D) spectrum and wave statistics were computed on an onboard microprocessor and the data were transmitted to a shore-based computer via wireless communications. The original velocity time series were discarded. The transmitted statistics included buoy position, GPS time, mean period and direction, peak period and direction, significant wave height, and 1-D energy spectra. These data were sampled approximately every 30 min while the buoy was deployed. The data was accessed at the web address, http://cordc.ucsd.edu/projects/wavebuoys/.

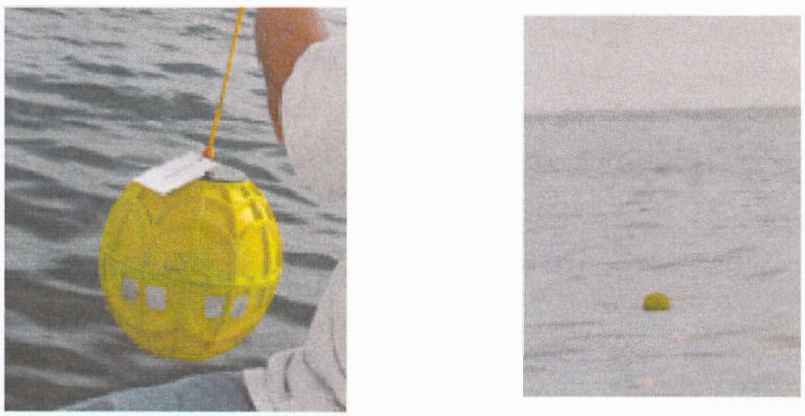

Figure 2. SIO miniature directional wave buoy.

6. Environmental Sensors

Tidal and wind data were obtained from the National Oceanic and Atmospheric Administration (NOAA) station #9410230 located at the end of the SIO peir, 32.867 deg north and 117.257 deg west. The wind speed and direction data were provided hourly, while the tidal data were in 6 min increments. The anemometer was located approximately 20 m above mean sea level. Tidal water level was referenced to the Mean Lower Low Water (MLLW) datum.

7. GPS

Two differential GPS units, Magellan ProMark 3.0, were utilized to determine precise differences in position between the radar antennas and the position of the Parker. These data were acquired at 1 Hz with differential vertical position accuracy of ±0.15 m (0.5 ft) over a ±5.56 km (3 nmi) range. Horizontal accuracy, when using differential corrections, is 50-70 cm.

8. Instrumentation Radar

This system was a calibrated linear FM homodyne X- and Ku-band coherent instrumentation radar, developed by Sensor Concepts Incorporated (SCI, Inc.) and referred to as the DREAM system. It was used for both the sea clutter and multipath measurements. The DREAM system transmitted all frequencies, $f_C \pm (\Delta f/2)$, simultaneously, and received the amplitude and phase of the return signal for all frequencies, allowing the measurement of Doppler (phase) shifts as well as calibrated RCS backscatter intensity. The DREAM system was dual-polarized (had both vertical-transmit and vertical-receive (VV), and horizontal-transmit and horizontal-receive (HH) polarizations) and was operated at pulse repetition frequencies (PRF) of 400–800 Hz. It covered spatial extents of 25–600 m at a resolution of 10–30 cm, much finer spatial resolution than was available from the WaMoS system (see 9.), but with much smaller range extent. The DREAM antenna was installed at the end of the SIO pier, as shown in Figure 3. During the experiments, it was approximately 14 m (46 ft) above the sea surface. The DREAM antenna did not rotate, thus the system collected 1-D radar range images in time.

Calibration of this radar was performed morning, noon, and evening each test day by measuring the RCS of a precision flat plate at a specially selected location that minimizes or eliminates any multipath from the calibration signal. This calibration site is shown in Figure 4.

9. Navigation Radar

A Furuno model 2117BB navigation radar was installed at the end of the SIO pier and was used for sea clutter measurements (Figure 3). The Furuno antenna was located approximately 24 m (78.7 ft) above MLLW, transmitted in X-band with HH polarization at a sampling frequency of 20 MHz, and had an antenna rotation period of ~1.5 s. The Furuno acquired 12-bit 2-D polar radar backscatter intensity images in time, and the data were collected within an 80 deg sector centered on the pier's heading. This sector was setup to minimize any interference between the Furuno and DREAM radar systems. The Furuno data were collected and automatically post-processed by the WaMoS II® ocean monitoring system (www.oceanwaves.org). The combined Furuno/WaMoS II® system is hereafter referred to as WaMoS.

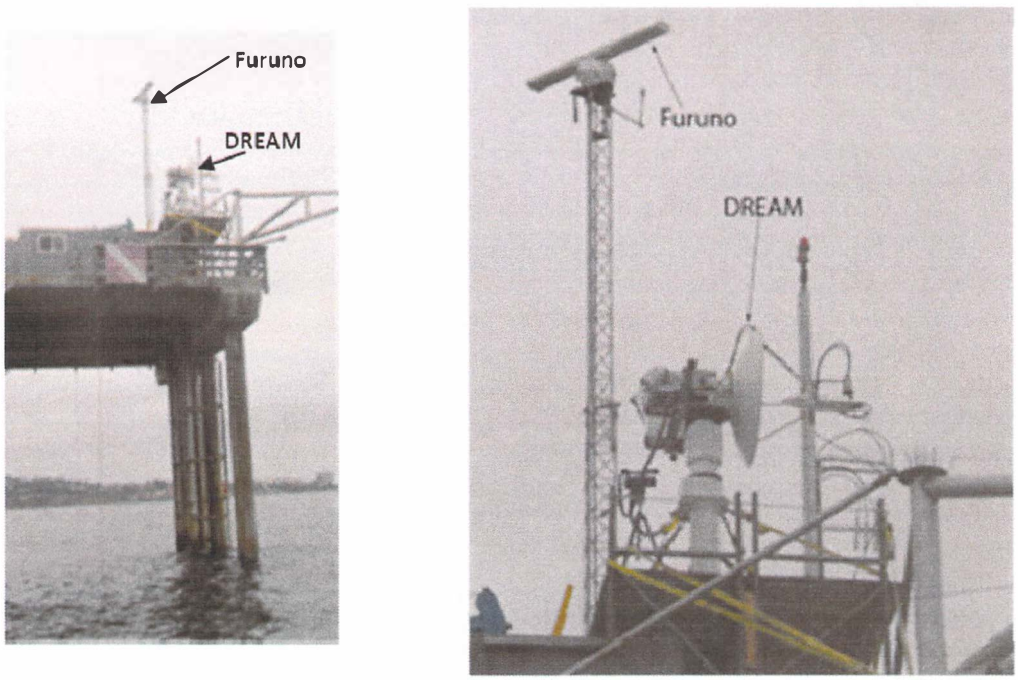

Figure 3. Radar setup at the end of the SIO pier.

SEA STATE MEASUREMENTS

Experiments were performed in the region just offshore the SIO pier, Figure 5, in La Jolla, CA from 26-30 July 2010. The 330.4 m (1084 ft) long SIO pier is oriented at 277 deg true. Characterization of multipath effects associated with ocean surface waves as well as the evaluation of the ability of radars to characterize these waves requires independent knowledge of the sea state, specifically wave statistics such as peak period, peak wave direction, mean period, frequency spectra, and significant wave height.

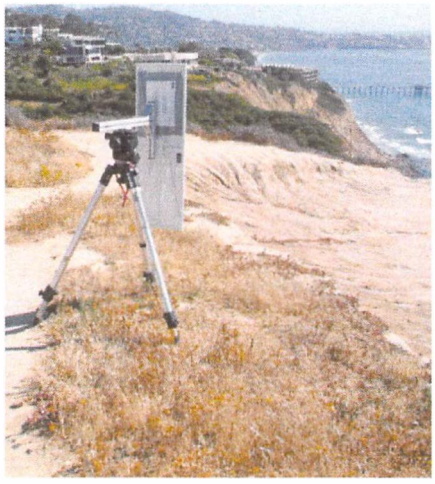

Figure 4. Calibration site and flat plate used for DREAM system calibration.

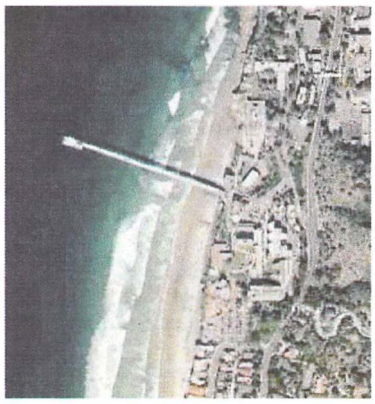

Figure 5. The SIO pier.

EXPERIMENTS

Two local, independent, measurements of the sea state were performed using conventional sensors. Multiple sensors allow evaluation of the temporal and spatial variability of the wave field. One local source was provided by the array of Senix ultrasonic distance sensors that were installed aboard the Parker. The second was provided by miniature directional wave buoys deployed from the Parker.

The 3 Senix ultrasonic probes were used to measure wave heights as the Parker drifted near the region of interest (i.e., the area illuminated by the radars). The data was corrected for ship motion using measurements performed by the IMU. Motion correction was performed by first converting measured roll and pitch accelerations to a fixed axis coordinate system. Next, double integrations of the vertical accelerations were computed to obtain heave displacement of the IMU and Senix sensors. Finally, Senix roll and pitch corrections were calculated relative to the IMU's position, and corrections for heave, roll, and pitch were added to the Senix data to obtain the final motion-corrected measurements. The motion corrected water level measurements were used to estimate directional wave spectra using a maximum likelihood method [2, 3] and/or a phase-path-time difference (PPTD) method [2, 4] from which various wave statistics were computed, including frequency spectra, significant wave height, and peak period. In addition, the 2 SIO miniature buoys were deployed from the Parker and drifted near the region of interest until recovered at the end of each test day. Tidal water level, wind speed, and wind direction data were also collected by a permanent measurement station located at the SIO pier.

SAMPLE RESULTS

The Senix array data were processed using the PPTD method of computing wave spectra, which uses differences in wave arrival times for gage triads to determine a mean wave direction for each frequency [2, 4]. Integration over all directions results in an estimate of the 1-D energy spectrum as a function of frequency. A sample spectrum along with the buoy-measured spectrum at a similar time is shown in Figure 6.

The Senix measurements extend to higher frequencies than the buoy data, which is limited by the diameter of the buoy itself for measuring high frequency oscillations. Conversely, the Senix data are limited at low frequencies due to boat drift; too much change in boat heading introduces error into the computation of the directional spectra. The increase in energy at low frequencies for the buoy data is associated with drift and changing of GPS satellites, which results in an apparent low frequency signal that should be neglected.

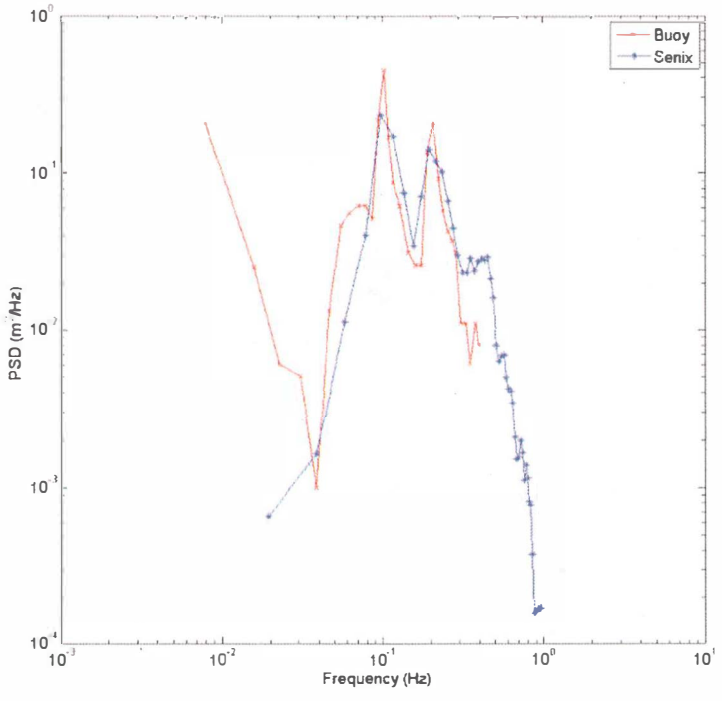

Figure 6. Sample Senix array and buoy spectra taken at a similar time period.

MULTIPATH MEASUREMENTS

As discussed in the Introduction, the secondary objective of these tests was to acquire data suitable to study multipath physics. Multipath refers to the propagation of electromagnetic waves between the antenna and target through multiple paths, which constructively and destructively interfere with each other.[1] For horizontal polarization at low grazing angle over a perfectly smooth and perfectly conducting surface, the analytical relationship for the ratio of the signal power density received at the radar relative to that in free space is [5]:

$$\eta^4 = 16\sin^4(2\pi HH_t / \lambda_r R) \quad (1)$$

where, η is the field strength ratio between that in the presence of a surface and that in free space, H is the height of the antenna, H_t is the height of the target, λ_r is the radar wavelength, and R is the range between the antenna and the target. These multipath (MP) effects result in the constructive and destructive interference pattern shown in Figure 7.

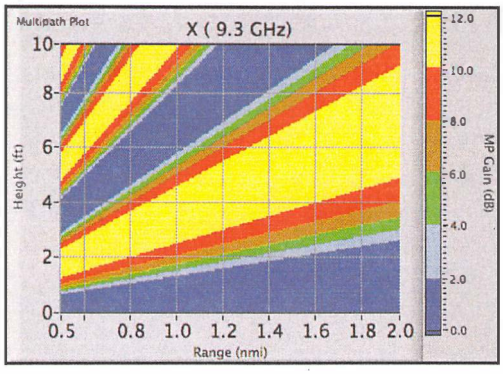

Figure 7. Theoretical multipath (MP) curve for HH X-band.

However, the ocean surface is not smooth and consequently the pattern of interference is much less predictable. Various statistical models (e.g., Gaussian, Rayleigh, log-normal) of sea clutter have been proposed, but none are able to replicate all the observed features of backscatter from the sea surface at low grazing angles [5]. One of the more widely used models of multipath that attempts to account for surface roughness effects is the "Miller-Brown" model proposed by Miller, Brown, and Vegh in 1984 [6]. This model assumes the sea surface is composed of a Gaussian collection of sinusoidal surface waves with uniform phase distribution. To improve upon such models, this portion of the test focused on measuring received signal power density from a known reflector over various ocean surfaces in an effort to better understand multipath physics for time-dependent, inhomogeneous rough surfaces.

EXPERIMENTS

For these tests, the instrumentation radar was used to measure the RCS of a pair of trihedrals, one at ~1 m (3 ft) above the water surface and the other at ~2 m (6 ft), mounted on the Parker as it drove inbound toward the radar. In addition, two differential GPS units were operated. One was set-up at the base of the DREAM antenna at the end of the pier, and the other unit was on the Parker. This configuration allowed the relative distance between the radar and the small boat to be measured with

[1] Ideally, there are 4 paths, which can result in total cancellation of radar return power or amplification of the return power by up to 16 times the free-space return power, depending on their relative phases.

high precision. Senix sensors were also positioned at the same location as each trihedral to measure the instantaneous height of each trihedral above the sea surface. Figure 8 shows this experimental setup.

The Parker, rigged with the trihedrals, was driven inbound at approximately 2.6 m s^{-1} (5 knots) towards the pier from specified waypoints. Each path was approximately 2.78 km (1.5 nmi) long. The Senix array measured the height of each trihedral above the water surface as the boat was underway, and the DREAM system range-tracked the Parker and the trihedrals over the course of each run. Table 1 summarizes the multipath runs performed during the test period, and Table 2 lists the parameters of the DREAM radar for these runs. In total, about 2 hours and 10 min of multipath data were collected.

Although the variation in sea state was not large, multipath runs were performed under as large a range of environmental conditions as possible for this time period and location. Figure 9 shows the wind speed and direction over the course of the test period, and the blue diamonds indicate the times of the multipath runs. Table 3 summarizes the environmental conditions for each of the corresponding multipath tests as measured by one of the miniature wave buoys deployed from the Parker and the anemometer. The other buoy shows similar results. The closest environmental measurements to that of the radar data are shown, and these times are noted in the table.

Table 1. Summary of multipath test runs.

Date	Time (UTC)	Duration (min)	DREAM Run Number
7/27	20:11	20	243
7/27	21:04	19.7	245
7/27	21:54	19.4	249
7/28	18:09	17.6	253
7/28	21:57	17.3	261
7/29	17:22	17.25	266
7/29	20:47	19	271

Table 2. DREAM radar configuration for multipath runs.

Logical Radar Title	LR0	LR1	LR2	LR3
Band and Polarization	X, HH	X, VV	Ku, HH	Ku, VV
Frequency Steps	256	256	256	256
Center Frequency, f_c (GHz)	9.3	9.3	15.4	15.4
Bandwidth, Δf (GHz)	1.5	1.5	1.5	1.5
Resolution (m)	0.10	0.10	0.10	0.10
Range Extent (m)	25.6	25.6	25.6	25.6
PRF (sweeps s^{-1})	400	400	400	400
#Integrations	0	0	0	0
Doppler(±m s^{-1})	3.24	3.24	1.95	1.95
Expected NERCS (1.85 km - single frequency)	-1	-1	-1	-1
Expected NERCS (1.85 km -range resolved)	-25.0	-25.0	-25.0	-25.0
Sensitivity (1.85 km - 256 sweep Doppler NERCS)	-49.0	-49.0	-49.0	-49.0

SAMPLE RESULTS

A sample of the measured DREAM radar return signal is shown in Figure 10a. The color-scale shows RCS as a function of transmitted frequency and time (or burst number). The first post-processing step is to range-resolve the data by applying a discrete fast Fourier transform (FFT) across all

frequency steps (the horizontal axis in Figure 10a). The result of this FFT processing is shown in Figure 10b, which shows RCS versus range and time. This procedure is referred to as range-resolving the data, and the data as presented in Figure 10b is referred to as a downrange profile history (DRPH). Only after range-resolving the data is the presence of six discrete scatterers apparent. The scatterers are moving toward the radar, which is evident by the decrease in range for increasing time (burst number).

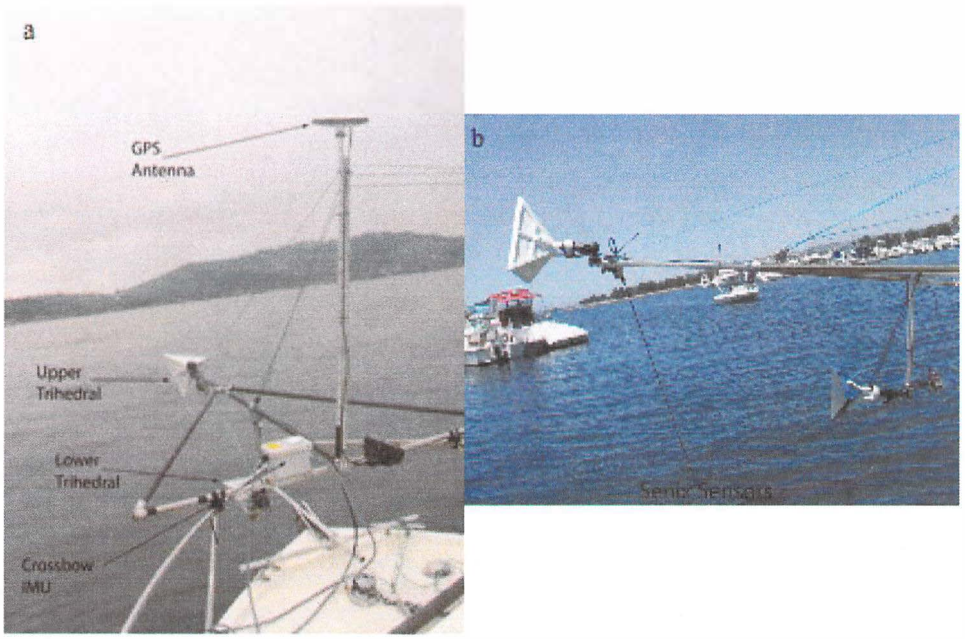

Figure 8. (a) Trihedral configuration on the small boat and position of the GPS and IMU sensors. (b) Profile view of the trihedrals and position of Senix sensors.

Table 3. Environmental conditions during multipath test runs, where H_s is significant wave height, $\overline{T}$ is mean wave period, T_p is peak wave period, θ_p is peak wave direction, θ_W is wind direction, and U_w is wind speed.

Run	Date	Radar Time (UTC)	Buoy Time (UTC)	H_s (m)	$\overline{T}$ (s)	θ_p (degT)	T_p (s)	Wind Time (UTC)	θ_W (degT)	U_w (m s^{-1})
243	7/27/2010	20:11	21:03	0.59	7.1	281	9.8	20:20	303	3.1
245	7/27/2010	21:04	21:03	0.59	7.1	281	9.8	21:20	297	3.9
249	7/27/2010	21:54	22:04	0.6	6.3	281	9.1	22:20	298	5.2
253	7/28/2010	18:09	18:01	0.65	6.7	283	4.5	18:20	345	3.8
261	7/28/2010	21:57	22:04	0.64	6.8	252	9.1	22:20	294	3.7
266	7/29/2010	17:22	18:31	0.59	5.6	285	4.8	17:20	352	2.0
271	7/29/2010	20:47	21:04	0.62	5.1	296	5.2	20:20	296	3.9

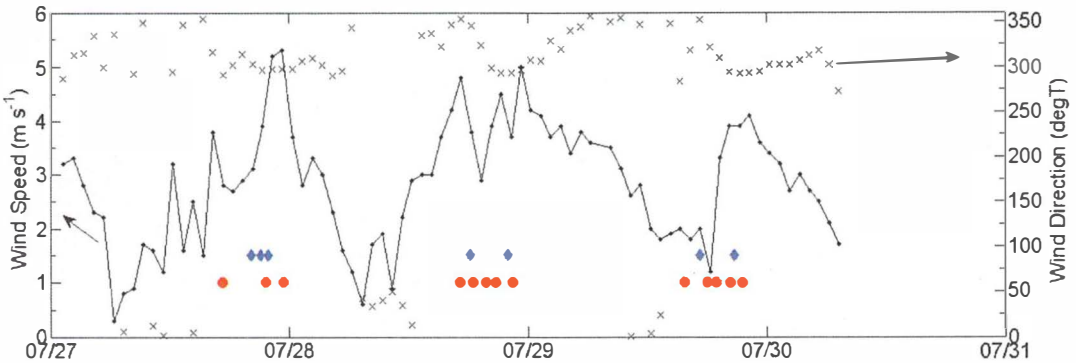

Figure 9. Wind speed and direction during the test period. Blue diamonds indicate times of multipath test runs, and red circles sea clutter runs.

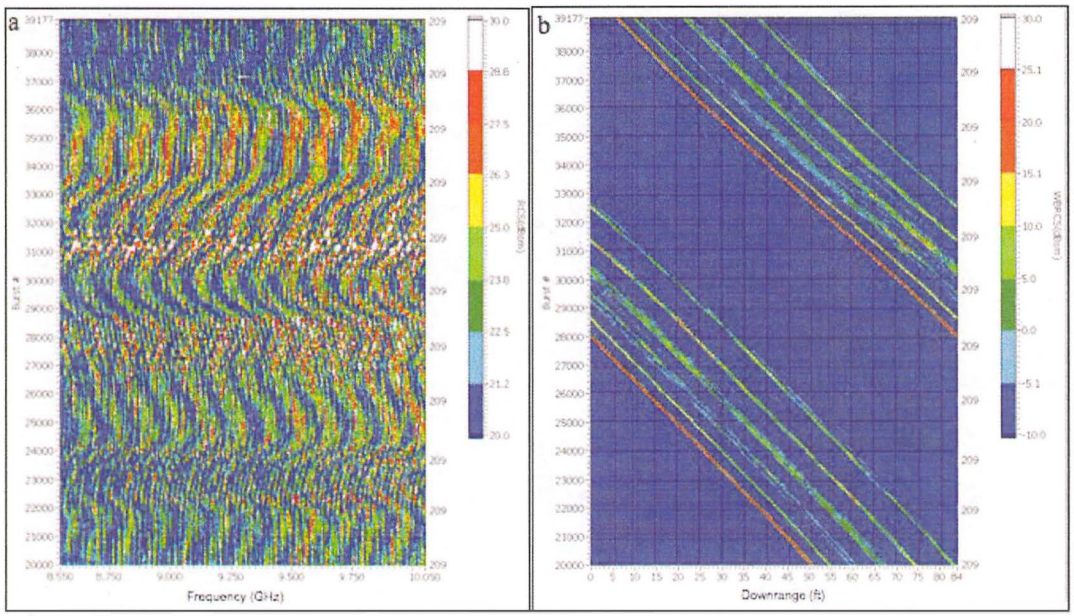

Figure 10. (a) Sample RCS versus frequency and burst number (time). (b) The same data after application of FFT along the frequency axis in order to range-resolve the data.

Multipath analyses require that the RCS of the trihedrals as a function of space and time be extracted from the acquired radar data. An example DRPH for a multipath run is shown in Figure 11. As the small boat moves-in in range, it wraps around the resolved range cells. For example, take a target moving from the furthest range cell at 25.6 m (84 ft) to the first range cell (note these cells are referenced to the range position of the entire window) — after moving through the 0 m range bin, the target wraps back around to the 25.6 m (84 ft) range cell and moves through the entire range window again. This wrapping results in the DRPH in Figure 11 having a checkerboard type appearance (wrapping is more clearly observed in the magnified DRPH shown in Figure 10b). Thus, in order to identify and separate the trihedrals in the radar return signal, the DRPH must be unwrapped and then motion compensated. The latter is required because the boat was not moving at a constant velocity, thus the unwrapping procedure does not result in the trihedrals falling in the same range bin for each

pass through the range window. The result of unwrapping and motion compensating the DRPH is shown in Figure 12. The motion compensated DRPH clearly shows several distinct scatterers that are now aligned within the same range bin over time. The first two scatterers on the left are the trihedrals, while the others are from features on the Parker. Note the significantly higher mean RCS level of the trihedrals relative to the others.

Example comparisons of measured trihedral RCS spatial variations for HH X-band data are shown in Figure 13. The height information was obtained from the Senix sensors. Each subfigure shows measured RCS distribution over range for selected trihedral heights along with theoretical and model predictions for those heights. Ultimately, the goal is to improve models of multipath over rough ocean surfaces, as well as to use them for correcting the RCS of sea clutter in an effort to improve wave height measurements obtained using radar backscatter.

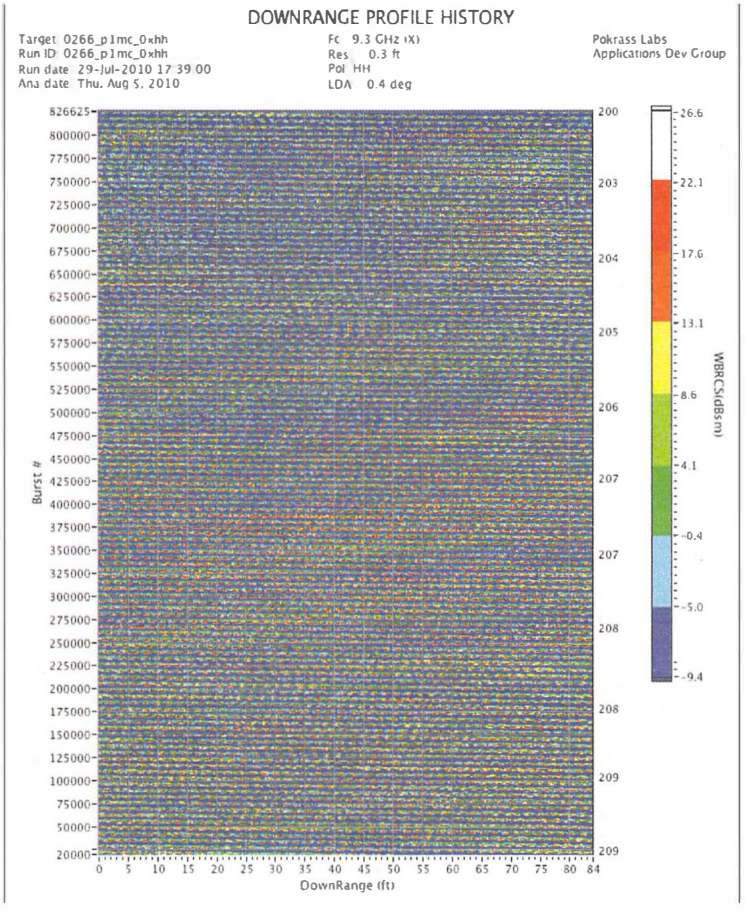

Figure 11. Downrange profile history for a sample multipath run.

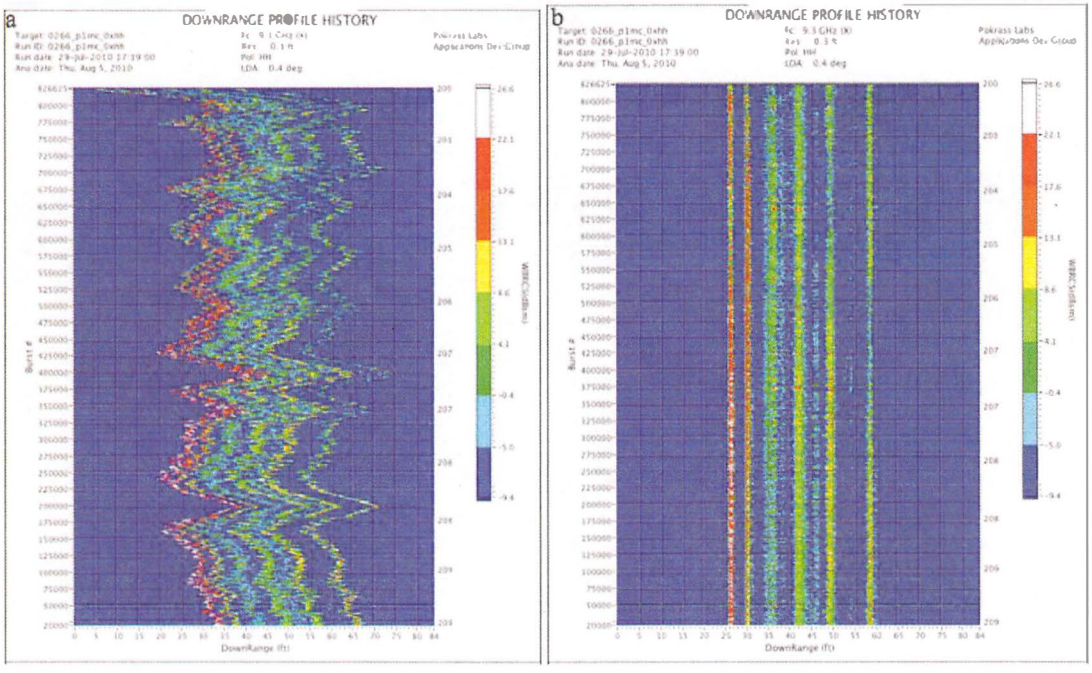

Figure 12. (a) Unwrapped downrange profile history (DRPH). (b) Unwrapped and motion compensated DRPH.

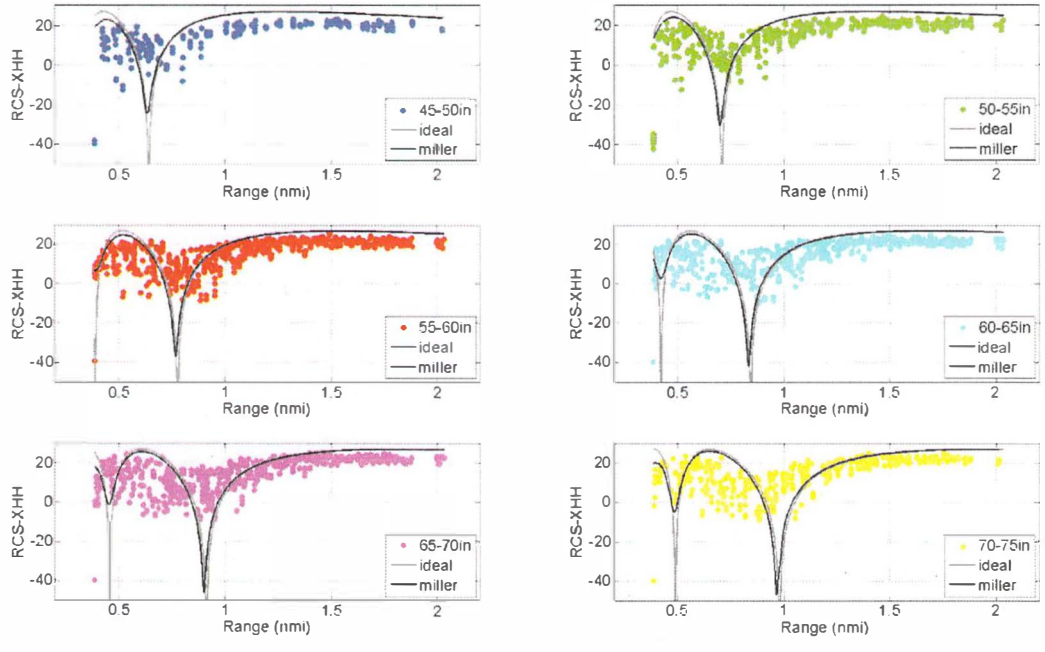

Figure 13. Comparison of measured multipath data (points) to theoretical multipath curves (gray lines) and the Miller-Brown multipath model (black lines) for several different trihedral heights above the sea surface.

SEA CLUTTER MEASUREMENTS

The primary objective of these tests was to obtain data to evaluate the ability of low-grazing angle radars to provide near-field, near-real time sea-state data suitable for enabling a high-fidelity ship control system to control ship motion during Sea Basing ship-to-ship logistic operations in Sea State (SS) 4 and below. To support this objective, radar backscatter from the sea surface was collected using both coherent and incoherent radar systems under as large a range of environmental conditions as possible at this location during the test period.

EXPERIMENTS

Sea clutter test runs were performed by aligning the DREAM radar azimuth along (and into) the wave propagation direction and collecting radar returns continuously for 10–20 min. The wave propagation direction was estimated by visual observation of the incoming wave field, and post-processing revealed that for most runs the DREAM radar azimuth was within 25 deg of the peak wave direction. The Parker, operating just outside the radar field-of-view, collected sea state data using the Senix array, and personnel aboard also deployed miniature directional wave buoys for determining the actual wave conditions at times and locations close to that of the sea clutter runs. In addition, the WaMoS system simultaneously collected data during many of the DREAM sea clutter runs. A summary of the DREAM sea clutter datasets are shown in Table 4 and the DREAM radar configuration for these runs is provided in Table 5. The last column of Table 4 indicates whether the WaMoS system was collecting data synchronously with the DREAM system. When data were not collected simultaneously, WaMoS data collection occurred just prior to or following the DREAM data collection. This procedure was adopted during testing to ensure we would obtain clean data sets if the interference between the radars was more significant than observed by a cursory review of data during testing. Figure 9 shows wind speed and direction along with the times of DREAM sea clutter runs. In total, about 3.5 hours of sea clutter data were collected.

Table 4. Summary of DREAM sea clutter test runs.

Date	Time (UTC)	Duration (min)	DREAM Run Number	WaMoS Data (Y/N)
7/27	17:18	10.25	236	Y
7/27	21:34	10.1	246	Y
7/27	23:26	10.27	250	Y
7/28	17:09	20.14	252	Y
7/28	18:29	10.4	254	N
7/28	19:47	20.3	258	N
7/28	20:43	15.24	259	N
7/28	22:30	22.4	263	Y
7/29	15:49	24.28	265	N
7/29	18:06	16.22	267	N
7/29	18:54	20.38	268	Y
7/29	20:22	10.34	269	N
7/29	21:38	21.6	272	Y

The WaMoS system processed data from a predefined analysis area within the operating sector of the radar. The location of this analysis box, as well as the average location of the DREAM range window is shown in Figure 14 along with the bathymetry[2] (and topography) of the test area. The average water depth in the area of the radar measurements was 48.4 m. This depth is near the deep water limit for surface gravity waves, but some of the longer wavelength swell would be considered within the

[2] Divins, D.L., and D. Metzger, NGDC Coastal Relief Model, http://www.ngdc.noaa.gov/mgg/ coastal/coastal.html. Download provided by the Southern California Coastal Ocean Observing System http://sccoos.org/data/bathy.

intermediate depth range. The WaMoS analysis area covered a square 960-m area at a spatial resolution of 7.5 m. Both the spatial range extent and resolution were much larger than that associated with the DREAM system (see Table 5).

Table 5. DREAM radar configuration for sea clutter test runs.

Logical Radar Title	LR0	LR1	LR2	LR3	LR4	LR5	LR6	LR7
Band and Polarization	X,HH	X,VV	Ku,HH	Ku,VV	X,HH	X,VV	Ku,HH	Ku,VV
Frequency Steps	2048	2048	2048	2048	2048	2048	2048	2048
f_c (GHz)	9.3	9.3	15.4	15.4	9.3	9.3	15.4	15.4
Δf (GHz)	1.5	1.5	1.5	1.5	0.5	0.5	0.5	0.5
Resolution (m)	0.10	0.10	0.10	0.10	0.30	0.30	0.30	0.30
Range Extent (m)	204.8	204.8	204.8	204.8	614.5	614.5	614.5	614.5
PRF (sweeps s^{-1})	800	800	800	800	800	800	800	800
#Integrations	0	0	0	0	0	0	0	0
Doppler($\pm$m s^{-1})	6.5	6.5	4.0	4.0	6.5	6.5	4.0	4.0
Expected NERCS (3.7 km - single frequency)	11	11	11	11	11	11	11	11
Expected NERCS (3.7 km - range resolved)	-22.0	-22.0	-22.0	-22.0	-22.0	-22.0	-22.0	-22.0
Sensitivity (3.7 km -256 sweep Doppler NERCS)	-46.0	-46.0	-46.0	-46.0	-46.0	-46.0	-46.0	-46.0

Table 6 lists relevant characteristics associated with the DREAM sea clutter runs including: distance to the first range bin (R), radar azimuth (θ_r), water level above MLLW (h), antenna height above the water surface (H), grazing angle (θ_g), and the difference between peak wave direction and radar azimuth ($\Delta\theta=|\theta_p-\theta_r|$). The peak wave direction was determined from miniature directional wave buoy #34, and h was determined from tidal station #9410230. In a few cases, the radar azimuth changed during the course of a run, and for those cases a range of values is provided in the table, but $\Delta\theta$ is based on the radar azimuth during the majority of the run. In one case, due to a system error, no azimuth data was recorded. Lastly, Table 7 summarizes the environmental conditions for each of the corresponding sea clutter tests as measured by one of the miniature wave buoys and the anemometer. The other buoy shows similar results. The closest environmental measurements to that of the radar data are shown, and these times are noted in the table.

SAMPLE RESULTS

A typical 2-D distribution of backscatter intensity measured by the WaMoS system is shown in Figure 15. The WaMoS system automatically post-processed this backscatter data for wave field statistics using procedures similar to those described in Story et al. [7] and Nieto Borge et al. [8]. Both the backscatter and post-processed data, which includes 1-D spectra, 2-D spectra, frequency-theta spectra, and wave statistics, were provided in separate files every 1–3 s. Individual spectra were computed from sets of 32 radar sweeps (~45 s), and mean spectra varied but could represent averages of up to 20 min.

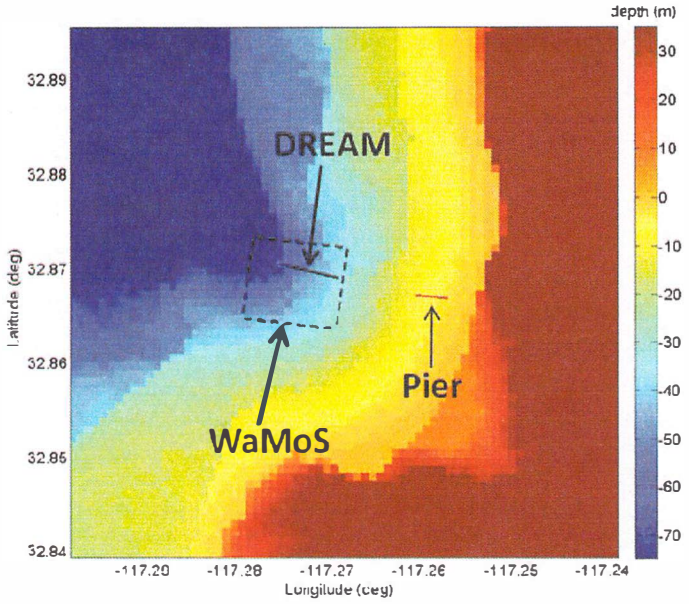

Figure 14. Bathymetry of the measurement area along with the average position of the DREAM range window and the location of the WaMoS analysis box.

Table 6. Relevant characteristics associated with DREAM sea clutter test runs.

Run	R (m)	θ_r (deg)	h (m)	H (m)	θ_g (deg)	$\Delta\theta$ (deg)
236	674.25	272	1.165	13.845	1.18	9.00
246	803.76	269.4	0.725	14.285	1.02	12.60
250	803.76	No data	0.536	14.474	1.03	N/A
252	803.76	295	1.065	13.945	0.99	18.00
254	915.28	295	1.218	13.792	0.86	67.00
258	915.28	275.65	1.135	13.875	0.87	12.35
259	915.28	275.86	0.974	14.036	0.88	44.86
263	803.76	283.15	0.612	14.398	1.03	31.15
265	803.76	267.9	0.649	14.361	1.02	17.10
267	791.78	283.55-280.94	1.172	13.838	1.00	4.06
268	803.76	285.33	1.250	13.760	0.98	0.33
269	815.77	300.95-300.03	1.132	13.878	0.97	4.95
272	806.17	317.51	0.910	14.100	1.00	21.51

Figure 16 shows typical DRPH measured by the DREAM system for X-band VV and HH polarizations. The horizontal streaks, particularly for the HH return, are due to interference from other radars that were operating in the vicinity. An increase in the amount of structure along range for VV relative to HH is apparent. The sloped lines in the figure are due to propagation of waves through the range window over time. Their slope is the phase speed of the waves.

Table 7. Environmental conditions during sea clutter test runs. See Table 3.

Run	Date	Radar Time (UTC)	Buoy Time (UTC)	H_s (m)	$\overline{T}$ (s)	θ_p (degT)	T_p (s)	Wind Time (UTC)	θ_W (degT)	U_w (m s^{-1})
236	7/27/2010	17:18	21:03	0.59	7.1	281	9.8	17:20	291	2.8
246	7/27/2010	21:34	21:34	0.6	7	282	9.8	21:20	297	3.9
250	7/27/2010	23:26	22:35	0.59	6.2	281	9.8	23:20	298	5.3
252	7/28/2010	17:09	17:31	0.63	7.1	277	4.8	17:20	353	4.8
254	7/28/2010	18:29	18:32	0.63	6.9	228	10.7	18:20	345	3.8
258	7/28/2010	19:47	20:03	0.65	6.2	288	4.8	19:20	324	2.9
259	7/28/2010	20:43	21:04	0.63	7	231	9.8	20:20	299	3.9
263	7/28/2010	22:30	22:04	0.64	6.8	252	9.1	22:20	294	3.7
265	7/29/2010	15:49	18:31	0.59	5.6	285	4.8	15:20	284	2.0
267	7/29/2010	18:06	18:31	0.59	5.6	285	4.8	18:20	323	1.2
268	7/29/2010	18:54	18:31	0.59	5.6	285	4.8	19:20	311	3.3
269	7/29/2010	20:22	21:04	0.62	5.1	296	5.2	20:20	296	3.9
272	7/29/2010	21:38	21:04	0.62	5.1	296	5.2	21:20	294	3.9

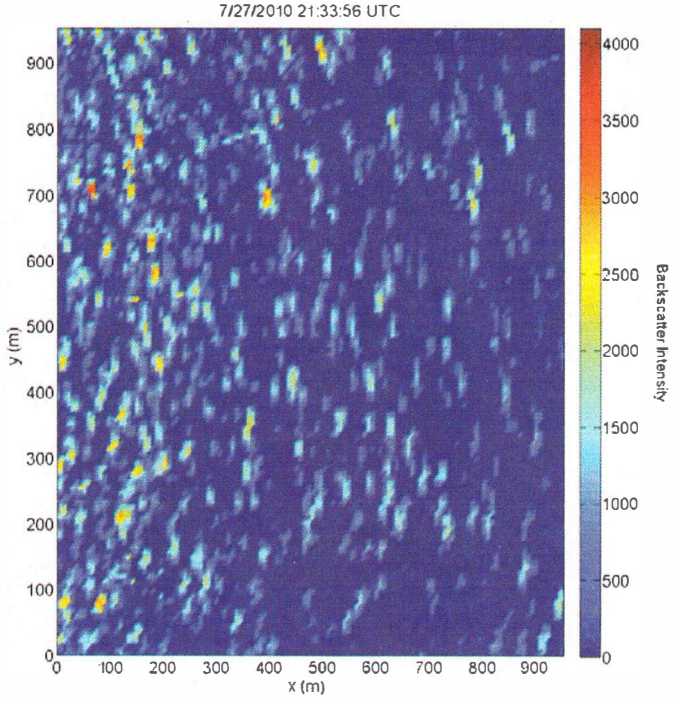

Figure 15. Sample WaMoS backscatter intensity (12-bit) map. The x-direction is equivalent to the range direction for the DREAM data.

The DREAM system measured phase variation in time was used to determine the Doppler velocity distribution. The standard way of computing Doppler distributions is by applying an FFT over time to the (complex-valued) DRPH [9]. A typical measured distribution is shown in Figure 17. A mean velocity of about 1 m s^{-1} towards the pier is evident. This offset contains a number of contributing factors including phase speed of capillary waves and currents of all sources; however, a thorough understanding of the sources of this offset remains a topic of current research. Variation about the mean value is also evident, which is primarily attributed to orbital velocities of the long surface gravity waves, but also contains other unsteady contributions such as phase speed of breaking waves [10].

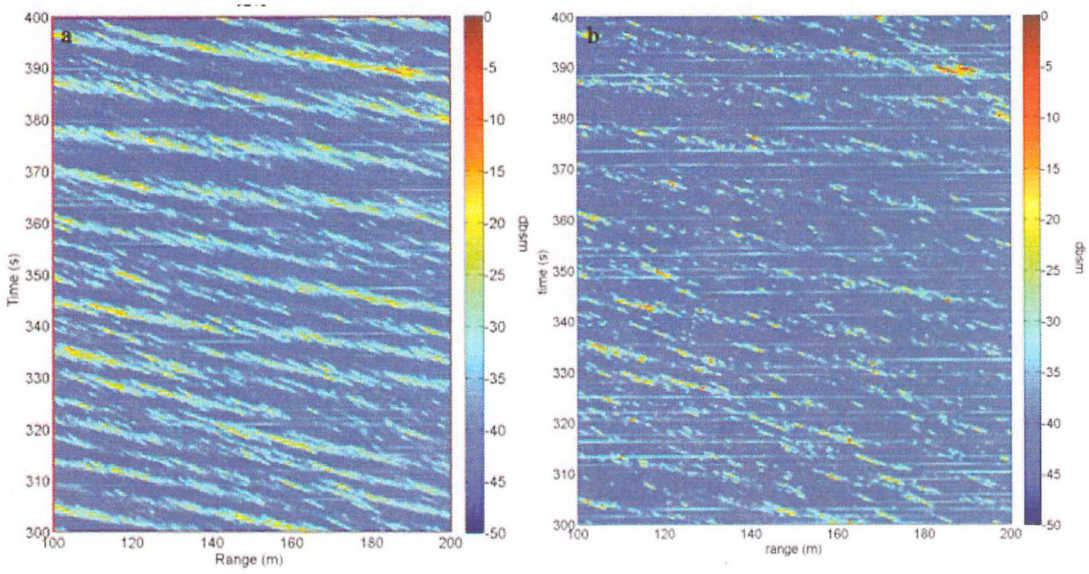

Figure 16. Sample DREAM DRPH of sea clutter for X-band (a) VV polarization and (b) HH polarization. Both examples are within 10 min of the sample data shown in Figure 15.

Doppler velocities can also be computed using pulse-pair processing [9, 11, 12]. This approach provides an estimate of the mean Doppler velocity for each range bin rather than the distribution shown in Figure 17. A sample result is provided in Figure 18, where any trend along range has been removed. Note that the sign convention is opposite that of Figure 17, i.e., positive velocities are towards the radar (SIO pier). The majority of the values are well within ±0.5 m s^{-1}, which is typical of orbital velocity values. Larger velocities are also sparsely present, which could be associated with phase speed of breaking waves and/or phase speed of smaller meter-scale waves [10, 13]. As demonstrated in Hackett et al. [11], these velocity distributions are used to compute velocity spectra, and subsequently converted to sea surface elevation spectra using linear wave theory in order to obtain radar-based wave field statistics. Sample comparisons of wave height spectra obtained from the post-processed WaMoS data and DREAM Doppler data along with that measured by the Senix array and a miniature wave buoy is shown in Figure 19. (Future reports will provide further details on comparisons of spectra and wave statistics from different sources, as well as details on the processing algorithms.)

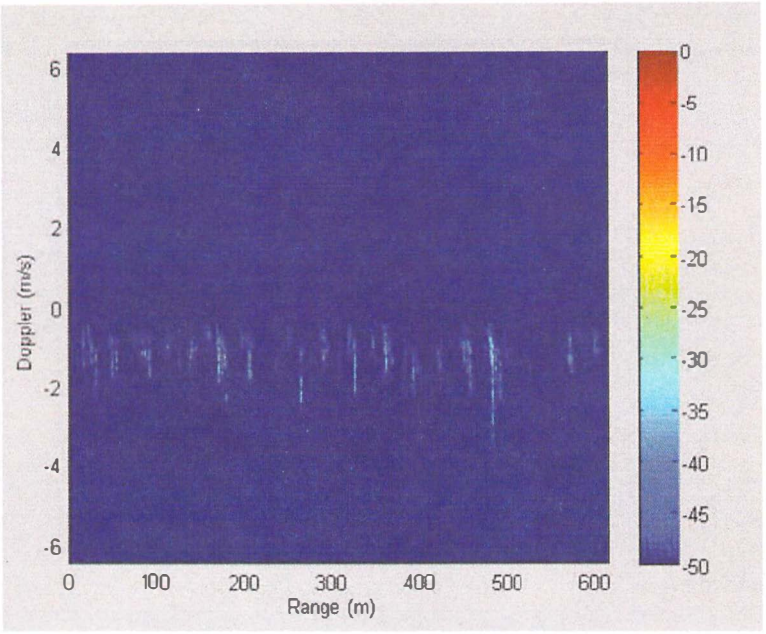

Figure 17. Sample X-band VV Doppler velocity distribution along range; color scale is in dBsm. The data is from the same time periods as Figures 15 and 16. Negative velocities are towards the radar (SIO pier).

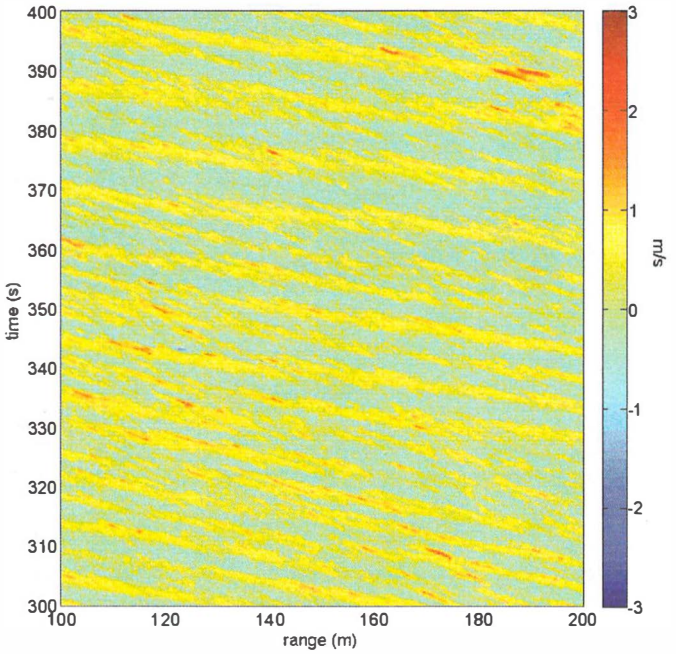

Figure 18. Sample distribution of mean X-band VV Doppler velocity. Note any trend or offset along range has been removed and positive velocities are towards the radar (SIO pier).

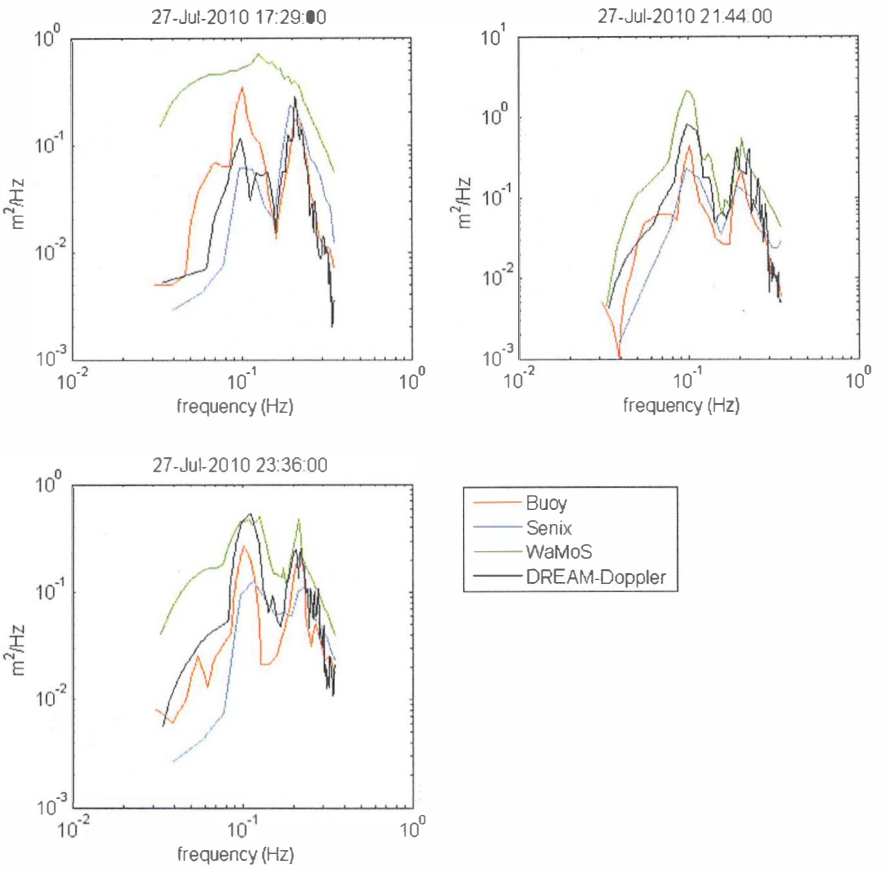

Figure 19. Sample comparisons of 1-D wave height spectra measured by the various sensors.

ONGOING AND FUTURE RESEARCH

The data described in this report, which were acquired during field experiments performed in July 2010, are currently being analyzed as part of research on several different topics. First, comparisons between the WaMoS and DREAM sea clutter data are being used to understand the impact spatial and temporal resolution have on the quality of retrieved wave statistics. Second, multipath data and sea-clutter data are being used to evaluate how large a contribution multipath is making to the sea clutter signal, how it can be removed, and what impact removing it would have on the accuracy of derived wave statistics. Third, DREAM sea clutter data is being analyzed to investigate alternative approaches for extraction of wave information from radar data using both coherent and incoherent signals. This effort includes evaluating whether incorporation of coherent return signals yields improved accuracy and reliability in comparison to using only incoherent measurements. Furthermore, this data is being used to improve our understanding of both coherent and incoherent backscatter from the sea surface. Lastly, the multipath data is being utilized to improve multipath models over rough ocean surfaces. The reader should look for future reports on these topics.

REFERENCES

[1] Izquierdo, P., C. Guedes Soares, J. C. Nieto Borge and G. R. Rodriguez (2004), A comparison of sea-state parameters from nautical radar images and buoy data, *Ocean Engineering*, 31:2209–2225.

[2] Fu, T. C., A. M. Fullerton, E. E. Hackett and C. F. Merrill (2011), Shipboard measurement of ocean waves, *Proc. ASME 30th International Conference on Ocean, Offshore and Arctic Engineering*, Rotterdam, The Netherlands.

[3] Capon, J. (1969), High-resolution frequency-wavenumber spectrum analysis, *Proc. IEEE*, 57(8).

[4] Esteva, D. C. (1977), Evaluation of the computation of wave direction with three- gage arrays, U.S. Army Corps of Engineers Technical Paper No. 77-7.

[5] Skolnik, M. I. (2001), *Introduction to Radar Systems*, McGraw-Hill, 3rd Edition, p. 485.

[6] Miller, A. R., R. M. Brown and E. Vegh (1984), New derivation for the rough- surface reflection coefficient and for the distribution of sea-wave elevations, *IEE Proceedings H Microwaves Optics and Antennas*, 131(2):114–116.

[7] Story, W. R., T. C. Fu and E. E. Hackett (2011), Radar measurement of ocean waves, *Proc. ASME 30th International Conference on Ocean, Offshore and Arctic Engineering*, Rotterdam, The Netherlands.

[8] Nieto Borge, J. C., G. R. Rodriguez, K. Hessner and P. I. Gonzalez (2004), Inversion of marine radar images for surface wave analysis, *J. Atmos. Oceanic Tech.*, 21:1291–1300.

[9] Thompson, D. R. and J. R. Jensen (1993), Synthetic aperture radar interferometry applied to ship-generated internal waves in the 1989 Loch Linnhe experiment, *J. Geophys. Res.*, 98(C6):10259–10269.

[10] Hwang, P. A., M. A. Sletten, and J. V. Toporkov (2008), Analysis of radar sea return for breaking wave investigation, *J. Geophys. Res.*, 113(C02003), doi: 10.1029/2007JC004319.

[11] Hackett, E. E., A. M. Fullerton, C. F. Merrill and T. C. Fu (2011), Measurements of surface waves using low-grazing angle high-resolution pulse-Doppler radar, *Proc. ASME 30th International Conference on Ocean, Offshore and Arctic Engineering*, Rotterdam, The Netherlands.

[12] Hwang, P. A., M. A. Sletten and J. V. Toporkov (2010), A note on Doppler processing of coherent radar backscatter from the water surface: with application to ocean surface wave measurements, *J. Geophys. Res.*, 115(C03026), doi: 10.1029/2009JC005870.

[13] Plant, W. J. (1997), A model for microwave Doppler sea return at high incidence angles: Bragg scattering from bound tilted waves, *J. Geophys. Res.*, 102(C9) 21131–21146.

(THIS PAGE INTENTIONALLY LEFT BLANK)

DISTRIBUTION LIST

Copies		Name
NAVSEA		
1		DTIC
ONR		
3		Patrick Purtell (pdf only), Paul Hess III, Steven Russell
SAIC		
2		Don Wyatt, Kristy Beale, (pdf only)
SIO		
1		Eric Terrill (pdf only)
SCI		
1		Richard Pokrass (pdf only)
Division Distribution		
1	3452	Library (pdf only)
1	5040	Arthur Reed (pdf only)
1	5050	Thomas Fu (pdf only)
1	5800	Rae Hurwitz (pdf only)
3	5830	Erin Hackett, Anne Fullerton, Craig Merrill, (pdf only), Files (2)
1	5510	Christopher Bassler (pdf only)
2	7410	Shaun Simmons, Bruce Crock, (pdf only)
1	7310	Andrew Smith (pdf only)
1	7400	Sung Han (pdf only)